Materials Chemistry and Physics 267 (2021) 124711

Contents lists available at ScienceDirect

Materials Chemistry and Physics

journal homepage: www.elsevier.com/locate/matchemphys

Electronic, optical and thermodynamic characteristics of $Bi_{12}SiO_{20}$ sillenite: First principle calculations

M. Isik [a,*], G. Surucu [b,c], A. Gencer [d], N.M. Gasanly [b]

[a] Department of Electrical and Electronics Engineering, Atilim University, 06836, Ankara, Turkey
[b] Department of Physics, Middle East Technical University, 06800, Ankara, Turkey
[c] Department of Electrical and Energy, Ahi Evran University, Kirsehir, 40100, Turkey
[d] Department of Physics, Karamanoglu Mehmetbey University, Karaman, 70100, Turkey

HIGHLIGHTS

- $Bi_{12}SiO_{20}$ (BSO) compound was investigated by density functional theory calculations.
- The electronic, optical and thermodynamic characteristics of BSO were reported.
- The electronic band structure and density of state plots were presented in detail.
- The spectral dependencies of various optical parameters were plotted.

ARTICLE INFO

Keywords:
Sillenites
Density-functional theory
Thermodynamics
Optical properties
Semiconductors

ABSTRACT

$Bi_{12}XO_{20}$ (X: Si, Ge, Ti) ternary semiconducting compounds are known as sillenites and take a remarkable attention thanks to their attractive photorefractive properties. The present paper reports electronic, optical and thermodynamic characteristics of $Bi_{12}SiO_{20}$ by means of density functional theory (DFT) calculations. The crystalline structure of the compound was revealed as cubic with lattice constant of 10.135 Å. XRD pattern obtained from DFT calculations were compared with experimental data and there is a good consistency between them. The electronic band structure and density of state plots were presented in detail. The band gap energy of the compound was determined from electronic band structure and spectra of optical constants. The spectral dependencies of real and imaginary components of dielectric function, refractive index, extinction coefficient, absorption coefficient and loss function were plotted in the 0–12 eV spectral range. The revealed structural, electronic and optical characteristics were discussed taking into account the previously reported theoretical and experimental studies on the $Bi_{12}SiO_{20}$ sillenite.

1. Introduction

$Bi_{12}XO_{20}$ (X: Si, Ge, Ti) sillenite compounds have been attractive due to their various fascinating properties like photorefractive, photoconductivity, piezoelectric, optical activity [1–3]. These outstanding characteristics make them potential candidates for hologram recording, photocatalysts, signal processing, acoustic, image amplification, optical data processing and interferometry applications [4–7]. $Bi_{12}SiO_{20}$ (abbreviated as BSO) is one of the members of this sillenite family and have been a subject of interest due to its high electrical resistivity, wide band gap energy, high photorefractive sensitivity, high photocatalytic activity and long holographic storage times [8–10].

BSO belongs to *I*23 space group and crystallizes in cubic structure with lattice parameter of $a = 1.0105$ nm [8]. In the crystalline structure, SiO_4 tetrahedra locates on the corners and at the cube center while each Bi-atom is surrounded by seven O-atoms. Fig. 1 represents the crystal structure of BSO compound. BSO has been investigated theoretically and experimentally to get detailed information about its characteristic applications and potential usage applications. Theoretical studies presented the energy band structure and bonding properties [11,12], Raman frequencies [8], energetic properties of antisite defects [13] and elastic properties of BSO [14]. Experimental studies revealed the various structural, optical, electrical and photocatalytic properties of the compound. X-ray diffraction pattern of BSO single crystals presented seven

* Corresponding author.
E-mail address: mehmet.isik@atilim.edu.tr (M. Isik).

https://doi.org/10.1016/j.matchemphys.2021.124711
Received 25 November 2020; Received in revised form 14 April 2021; Accepted 2 May 2021
Available online 6 May 2021

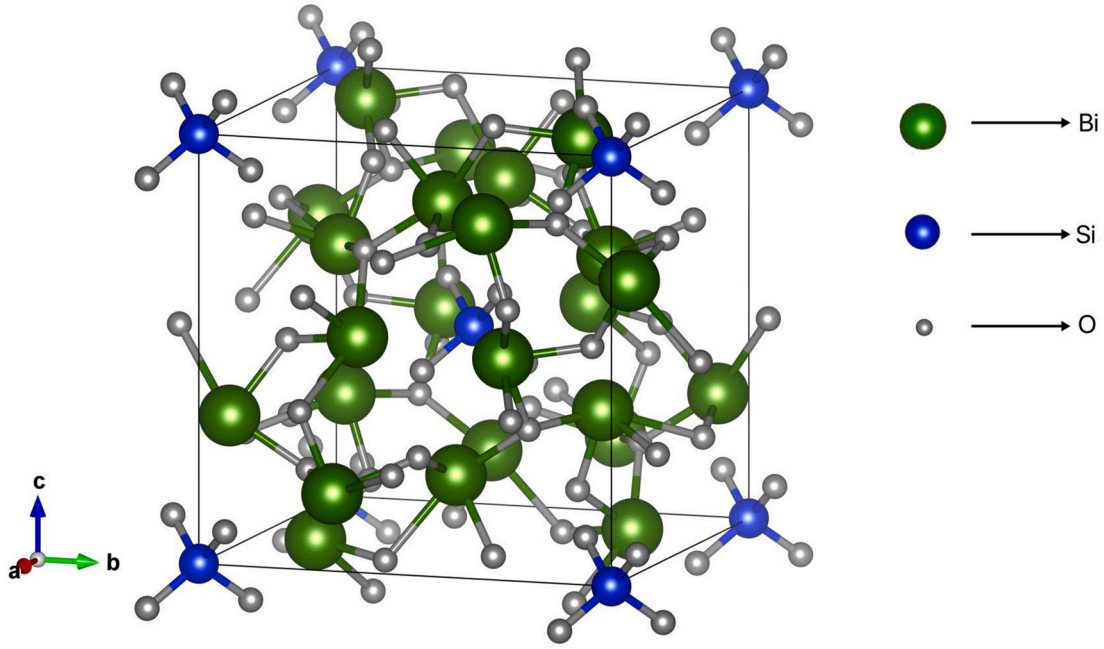

Fig. 1. Crystal structure of $Bi_{12}SiO_{20}$ sillenite.

diffraction peaks associated with cubic crystalline structure [9]. Two different band gap energies were reported for BSO compound; one of them is around 2.3 eV and other one is around 3.2 eV [15–17]. The reason of large unaccepted difference between these calculated and/or determined energy values was explained taking into account the defect centers in BSO [18,19]. Members of $Bi_{12}XO_{20}$ sillenite family are known as defective materials and defect centers in the compounds take a remarkable role in the absorption processes. The critical point energies of 3.54, 4.02, 4.82 and 5.58 eV were reported from the analyses of ellipsometry measurements [9]. The spectral dependencies of various

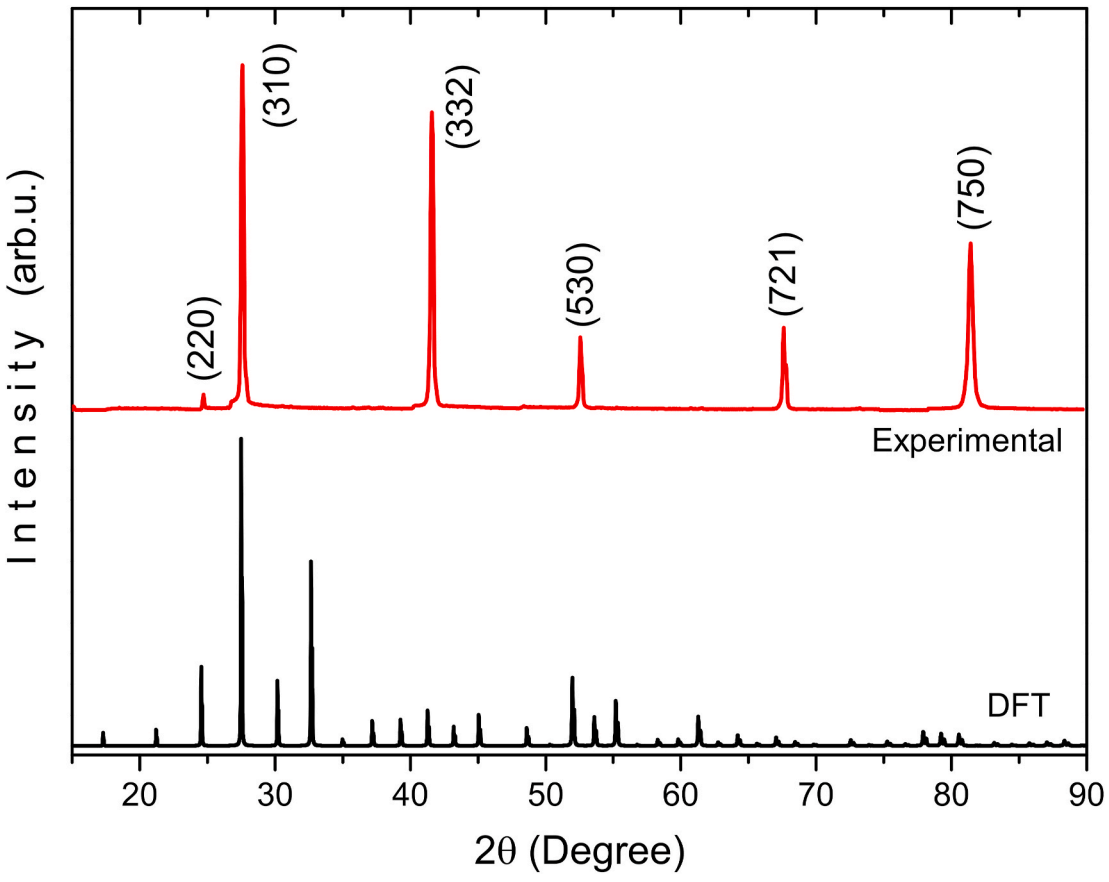

Fig. 2. XRD pattern of $Bi_{12}SiO_{20}$ obtained from DFT calculations and experimental data.

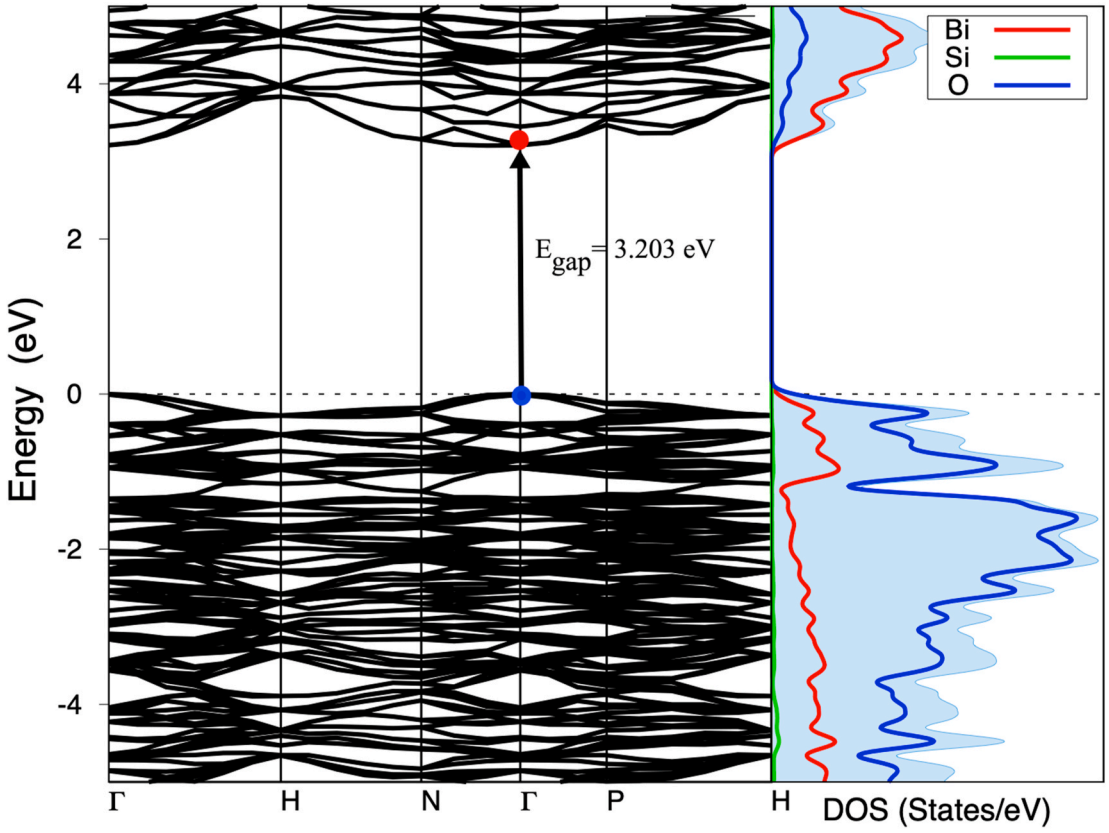

Fig. 3. Electronic band structure and partial density of state plots of $Bi_{12}SiO_{20}$ calculated with HSE06 method.

optical constants were also drawn in the 1.2–6.2 eV spectral range. BSO material exhibits p-type conductivity and has electrical resistivity of 5.0 $\times$ 10^{13} Ω cm and electron mobility of 4.5 $\times$ 10^{-3} $cm^2V^{-1}s^{-1}$ [20].

Although theoretical studies have presented various characteristics of the BSO, there are still unrevealed properties of the compound. The aim of the present paper is to investigate electronic, optical and thermodynamic properties of the BSO by means of density functional theory (DFT) calculations. Electronic band structure and density of states were plotted and lattice parameter of the compound was determined. Spectral dependencies of complex dielectric function, refractive index, extinction coefficient, absorption coefficient and loss function were reported for the first time as optical characterization of the ternary sillenite. Temperature and pressure dependent volume, thermal expansion and heat capacity values were plotted in the 0–20 GPa pressure and 0–1000 K temperature ranges. To the best of our knowledge, the calculated thermodynamic characteristics have not been reported up to now. The results of the present paper would remarkably provide valuable information to literature to look at the BSO sillenite in a detailed standpoint.

2. Calculation details

All the simulations in the present paper were performed by the self-consistent density functional theory (DFT) with a plane-wave pseudopotential approach implemented in the Vienna Ab-initio Simulation Package (VASP) [21,22]. The electron-ion interaction was considered with the Projected Augmented Wave (PAW) method [23]. The exchange-correlation functionals have been described using Perdew, Burke and Ernzerhof (PBE) [24] type pseudopotentials within the framework of generalized gradient approximation (GGA) based on density functional theory (DFT) [25] in which Kohn-Sham equations are solved numerically and iteratively [26,27]. Furthermore, the hybrid functional Heyd-Scuseria-Ernzerhof (HSE) method [28] is employed in order to prevent the underestimation resulted from the GGA-PBE method. For the HSE method, the screened HSE06 hybrid functional is taken with the screening parameter of 0.2 $Å^{-1}$ and 25% of the exact non-local Hartree-Fock exchange is mixed into the exchange part [29]. Also, the van der Waals interactions are employed to consider the non-bonding interactions [30]. The cut off energy for the plane waves was taken as 830 eV and a gamma centered grid [31] has been used to obtain k-points as 8 $\times$ 8 $\times$ 8 k-points since these parameters presented the optimum calculation results. Also, Methfessel–Paxton [32] type smearing method has been applied on fermionic occupation function with 0.01 eV smearing width. For the optimization process in which the atomic positions of the atoms in compositions are fully relaxed, the quasi-Newton technique has been performed until maximum force on each ion are smaller than 10^{-10} eV/Å. Also, iteration steps have been chosen 10^{-11} eV per unit cell to perform convergence for energy in successive iteration. Also, the thermodynamic properties are determined using the GIBBS code [33] with the density as 9.384 g/cm^3 and the Poisson's ratio as 0.275. Finally, the calculations based on the Bethe-Salpeter equation (BSE) [34,35] including the electron-hole interaction (excitonic effect) that is absent in DFT and GW approaches have been carried out to investigate the optical properties.

3. Results and discussions

3.1. Structural properties and electronic structure

BSO sillenite compound belongs to *I*23 space group and crystallizes in cubic structure. The optimization of the compound according to these structural characteristics has been successfully carried out. The calculations performed for structural characterization resulted in lattice parameter of $a = 10.135$ Å belonging to the cubic crystalline structure. This calculated lattice constant is well-consistent with reported value of $a = 10.107$ Å determined from analyses of experimental XRD pattern [9]

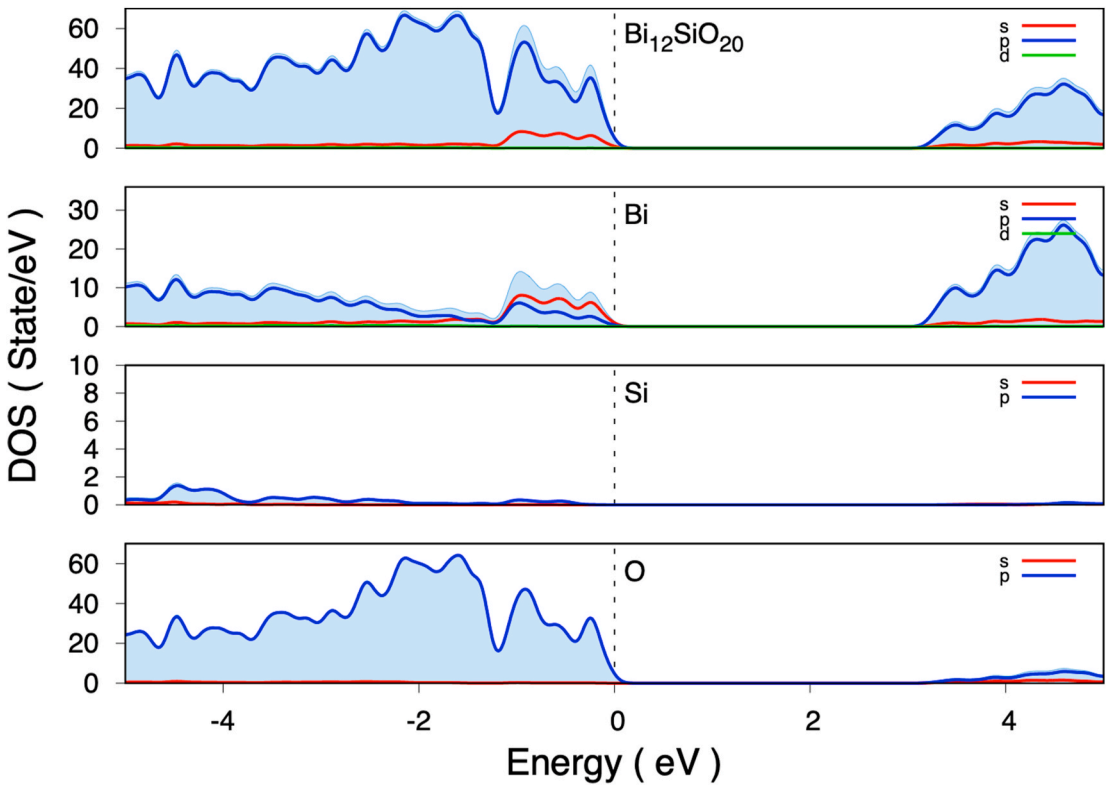

Fig. 4. Partial and total DOS plots of $Bi_{12}SiO_{20}$ calculated with HSE06 method.

and $a = 10.105$ Å [14] and 10.387 Å [36] calculated from theoretical studies. Fig. 2 indicates the XRD patterns obtained from DFT calculations and experimental studies [9]. The observed peaks in the experimental data are in good agreement with revealed pattern. The most intensive peak was observed around 27.50° corresponding to (310) plane. XRD diffraction peaks appear due to constructive patterns formed due to parallel planes. In Fig. 2, XRD pattern of bulk BSO crystal exhibited less diffraction peaks compared to that of calcuated pattern. The reason of observing a few peaks in bulk compounds is due to the fact of that the orientation of number of parallel planes in the bulk crystals is limited in the XRD experiments. However, theoretical DFT calculations are not restricted from this point and present more parallel planes.

The formation energy (ΔE_f) of BSO compound was calculated taking into account the following expression [37].

$$\Delta E_f = E_t(Bi_{12}SiO_{20}) - [12E_{Bi} + E_{Si} + 20E_O] \quad (1)$$

In Eq. (1), E_t symbolizes the total energy of the unit cell of BSO compound while E_X describes the ground state energy of one X atom (where X: Bi, Si, O) in its bulk crystalline form. The formation energy was calculated as −1.382 eV/atom. The negative formation energy is associated with thermodynamical stability behavior of the BSO compound that indicates the synthesizability of this compound.

Fig. 3 represents the electronic band structure and density of states (DOS) plots of BSO compound calculated with the HSE06 functional and Figs. S1 and S2 in the Supplementary File were calculated with the GGA-PBE method. As seen from Figure, valence band maximum and conduction band minimum are at the same point Γ in the Brillouin zone. The difference between them was calculated as 3.203 eV. Thus, this observation points out that BSO has direct band gap characteristics with a gap energy of 3.203 eV. However, the GGA-PBE method underestimates the band gap as 2.35 eV that can be seen from Fig. S1. The band gap energy of BSO was previously reported according to analyses of various experimental data. The analyses of ellipsometry [9] and transmission [15] experiments performed on BSO single crystals resulted in band gap energies of 3.25 and 2.48 eV, respectively. The absorption coefficient analyses presented the band gap energy as 2.2 eV in Ref. [17]. Also, the theoretical electronic band structure calculations presented the band gap energies as 2.85 eV with mBJ method and 1.91 eV with GGA-PBE method [36] and 2.42 eV with GGA-PBE method [11]. Our revealed band gap energy is well-consistent with values determined around 3.2 eV. The large difference between accepted energy of 3.2 eV and reported energies around 2.3 eV was explained in Ref. [38] taking into account the presence of intrinsic defect centers. A detailed investigation of effect of defects in $Bi_{12}MO_{20}$ (M: Ge, Si, Ti) sillenite crystals was previously accomplished using DFT calculations [13]. The electronic structures were calculated and DOS plots were reported for perfect and defective systems. The band gap energy of BSO (~3.2 eV) corresponds to the UV region. In Ref. [13], it was stated that visible light absorption by sillenite crystals is associated with Bi_M antisite defects and presence of defects reduces the band gap energy. Moreover, defect levels in BSO single crystals were investigated by thermoluminescence measurements [19]. The analyses of thermoluminescence glow curves pointed out the presence of a defect center around 0.81 eV [19]. Therefore, the calculated energies around 2.3 eV are associated with transition taking place between conduction band and defect center. It is known that semiconducting compounds with direct band gap energy are efficient photocatalysts since they have effective electron-hole excitation [39]. As it is known BSO exhibits fascinating photocatalysis characteristics.

DOS plot indicates the contribution of constituent atoms (Bi, Si, O) to the valence and conduction bands. As seen, O-atoms dominate valence band maximum while Bi-atoms dominate conduction band minimum. Fig. 4 represents the partial DOS plots in detail. The *p*-states of O-atoms provide the most remarkable contribution to the DOS between −5 and 0 eV. There exists a gap between 0 and 3.203 eV due to semiconducting characteristics of the BSO compound. Above the band gap energy region, *d*-states of Bi-atoms make significant contribution to the DOS. In addition, there are strong hybridizations between *p*-states of O, Si and Bi atoms in −5 to −3 eV while the strong hybridizations are occurred between *p*-states of O atoms and *s*-states and *p*-states of Bi atoms in −3 to 0 eV.

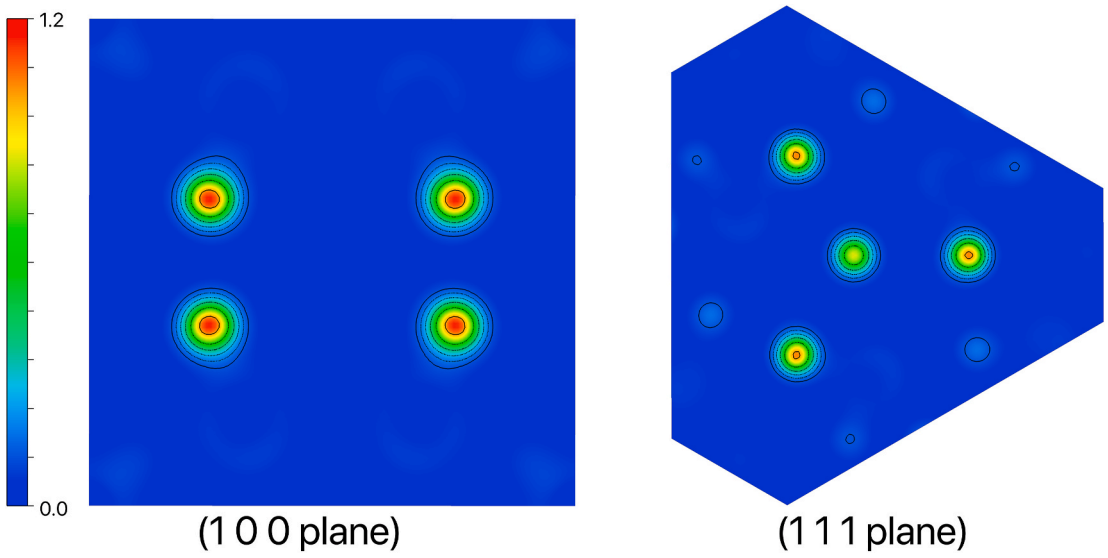

Fig. 5. Electron density distribution of $Bi_{12}SiO_{20}$ along the (100) and (111) planes.

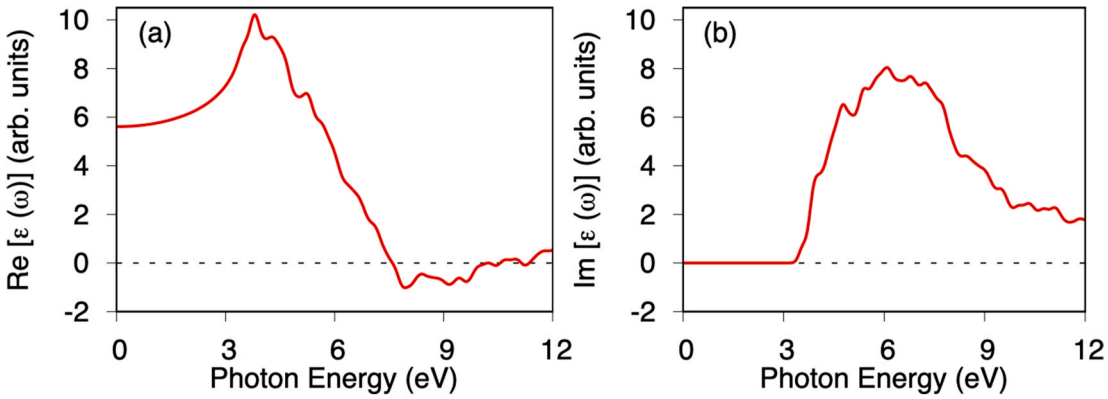

Fig. 6. Spectra of (a) real and (b) imaginary components of complex dielectric function.

The Bader partial charges were calculated for BSO using VASP and analyzed using the Bader charge analysis program [40]. The negative Bader partial charge indicates the charge transfer to the atom whereas the positive one indicates the charge transfer away from the atom. The BSO compound has 24 Bi atoms, 2 Si atoms and 40 O atoms in the primitive cell and the total Bader partial charge (in units of e) of Bi, Si and O atoms are 37.44, 3.82 and −41.28, respectively. So, the charge is transferred from Bi and Si atoms while the charge is transferred to the O atoms. Furthermore, Fig. 5 indicates the electron-density distribution for $Bi_{12}SiO_{20}$ compound along (100) and (111) planes. As seen from the figure, $Bi_{12}SiO_{20}$ sillenite exhibits dominantly ionic bonding characteristics. Also, the Poisson's ratio was obtained as 0.27 in Ref. [11] that also indicates the dominantly ionic bonding as consistent with the obtained electron density distribution in this study.

3.2. Optical properties

Spectral dependencies of various optical parameters of BSO were obtained from the frequency dependent dielectric function [41,42] and were plotted in the 0–12 eV range. Fig. 6 presents plots associated with real ($\varepsilon_{\text{real}}$) and imaginary ($\varepsilon_{img}$) components of dielectric function ($\varepsilon = \varepsilon_{real} + i\varepsilon_{img}$) obtained with HSE06 method. In addition, the real and imaginary parts of the dielectric function obtained with GGA-PBE method were plotted in Fig. S3. As seen from Fig. 6, the $\varepsilon_{\text{real}}$ decreases almost exponentially when the energy was decreased from 4.1 to 0.0 eV and intersects the $\varepsilon_{\text{real}}$-axis around 5.42. This observation states that low frequency ($\upsilon = 0$) dielectric constant of BSO is given as $\varepsilon_0 = 5.42$. The imaginary component takes zero below the ~3.332 eV. Since semiconductors are transparent below the E_g, ε_{img} is theoretically zero in the $h\upsilon < E_g$ region. Therefore, this energy is associated with band gap energy. The band gap values from the electronic band calculations (3.203 eV) and optical calculations (3.332 eV) are consistent. The critical point (CP) energy also called as interband transition energy refers to the energy difference between bands through which photons are transferred in the band structure. The peak positions in the ε_{img} spectrum are associated with CP energies [43]. The first four peaks were observed around 3.81, 4.02, 4.78 and 5.66 eV. In our previous paper, CP energies of BSO compound were determined from the analyses of spectroscopic ellipsometry data as 3.54, 4.02, 4.82 and 5.58 eV [9]. These energies show a very well consistency with peak positions in Fig. S3b.

The optical parameters of $\varepsilon_{\text{real}}$ and ε_{img} may be utilized to calculate refractive index (n), extinction coefficient (k), absorption coefficient (α) and loss function (L) using the following expressions [43].

$$n = \left[\left(\varepsilon_{real} + \left(\varepsilon_{real}^2 + \varepsilon_{img}^2\right)^{1/2}\right)/2\right]^{1/2} \quad (1a)$$

$$k = \left[\left(-\varepsilon_{real} + \left(\varepsilon_{real}^2 + \varepsilon_{img}^2\right)^{1/2}\right)/2\right]^{1/2} \quad (2)$$

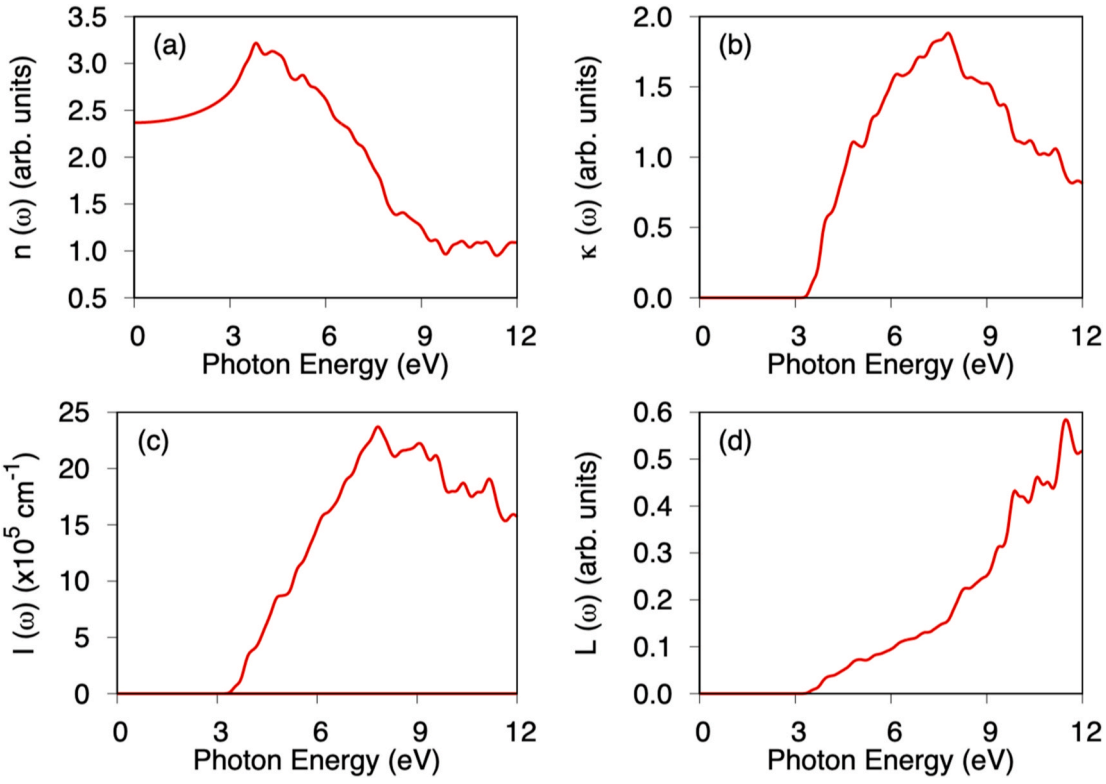

Fig. 7. Spectra of (a) refractive index (n), (b)extinction coefficient (κ), (c) absorption coefficient (I) and (d) loss function (L).

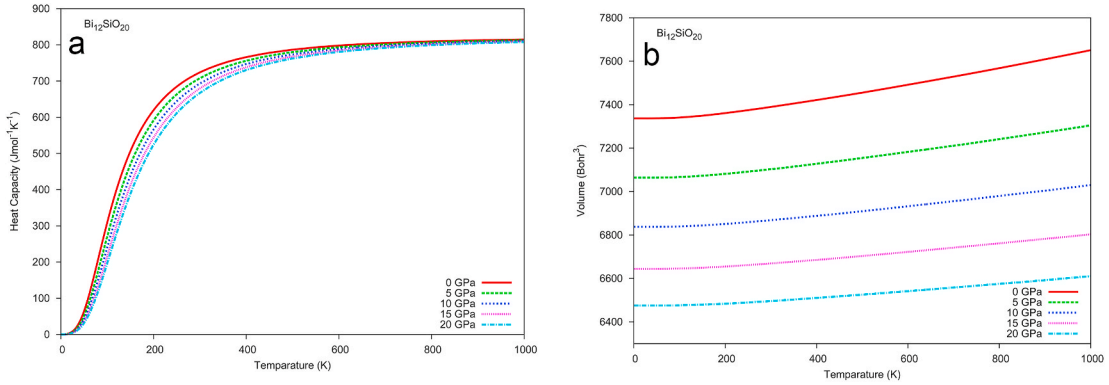

Fig. 8. Temperature-dependent (a) heat capacity and (b) thermal expansion coefficient at various pressures.

$$\alpha = \frac{4\pi k}{\lambda} \tag{3}$$

$$L = Im(-1/\varepsilon) \tag{4}$$

Fig. 7 indicates the spectra of plots taking into account the spectra of ε_{real}, ε_{img} and these equations obtained with HSE06 method and Fig. S4 shows the plots obtained with GGA-PBE method. The *n*-spectrum reveals the zero-frequency refractive index ($n(0)$) as nearly 2.33. The extinction coefficient behaves similarly with the imaginary part of the dielectric function and the extinction coefficient starts after the threshold energy as 3.306 eV and takes the highest value as 1.863 at 8.043 eV. The absorption coefficient takes values in the order of 10^5 cm^{-1} around the absorption edge. The high absorption coefficient value is associated with direct band gap energy characteristics of the BSO compound. This point supports the observed direct transition characteristics in the electronic band structure. The energy loss of a fast electron is represented with the loss function and as can be seen from Fig. 7, the loss function gets higher values for higher photon energies.

3.3. Thermodynamic properties

Thermodynamic characteristics of BSO compound was also calculated using quasi-harmonic Debye model [44]. Temperature dependent heat capacity (C_P) and thermal expansion plots were presented in Fig. 8a and b, respectively, at various pressures between 0 and 20 GPa. Heat capacity vs. temperature dependency exhibits exponential behavior and as temperature was increased above ~600 K, heat capacity reaches to the Dulong-Petit limit and gets value of ~820 J/(mol.K). Temperature vs. heat capacity behavior was previously investigated by experimental studies [45]. It was reported that as temperature was increased from 343 to 1093 K, heat capacity in a formula unit increases as an exponential behavior from 694 to 890 J/(mol.K). The high temperature heat capacities revealed in the present paper and in Ref. [45] may be thought as consistent with each other taking into account the applied research techniques and possible errors in present and Ref. [45] studies. In the

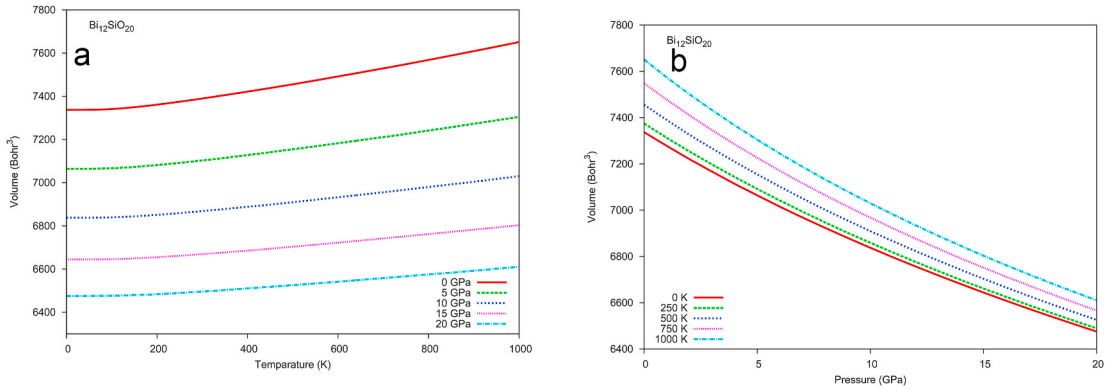

Fig. 9. (a) Temperature and (b) pressure dependent volume plots.

low temperature region, heat capacity exhibits T^3-dependency. Temperature dependent thermal expansion coefficient plots also exhibit exponential behavior. Thermal expansion coefficient increases rapidly in the $T < 200$ K region and increase above this temperature is rather slow. It is also seen from the plot that increase of pressure results in decrease in coefficient values.

Temperature and pressure dependent volume plots are presented in Fig. 9a and b, respectively. Unit cell volume is around 7380 $Bohr^3$ at room temperature and 0 GPa. Volume increases with temperature increment as expected. Volume depends remarkably on pressure as shown from Fig. 9b and volume-pressure dependency was observed as exponential.

4. Conclusion

Structural, electronic, optical and thermodynamic characteristics of $Bi_{12}SiO_{20}$ compound were investigated using density functional theory calculations. The crystalline structure of the material was found as cubic with lattice constant of 10.035 Å. The revealed negative formation energy of −1.382 eV/atom pointed out that BSO compound is thermodynamically stable. Total and partial density of state plots showed that *s*-states of O-atoms significantly contribute to the DOS in the bands below the valence band. Bi-atoms dominate in the conduction bands. Spectral dependencies of refractive index, extinction coefficient and complex dielectric function were presented throughout the paper. Band gap energy was determined as 3.203 eV from the electronic band structure with the HSE06 method and 3.306 eV from extinction coefficient spectrum. This wide direct band gap energy of BSO provides the compound a remarkable potential in photocatalysis and ultraviolet applications. The difference in between the band gap values determined from each calculation is due the BSE calculations in optical properties. The zero-frequency ($\nu = 0$) dielectric constant and refractive index were found as 5.42 and 2.33, respectively. Temperature and pressure dependencies of thermodynamic characteristics like heat capacity, thermal coefficient and unit cell volume were presented in detail.

CRediT authorship contribution statement

M. Isik: Conceptualization, Investigation, Formal analysis, Writing – original draft. **G. Surucu:** Investigation, Methodology, Formal analysis, Writing – original draft. **A. Gencer:** Investigation, Methodology, Formal analysis. **N.M. Gasanly:** Supervision, Writing – review & editing.

Declaration of competing interest

The authors declare that they have no known competing financial interests or personal relationships that could have appeared to influence the work reported in this paper.

Acknowledgement

This work was supported by ATILIM University under Grant No: ATÜ-ADP-1920-03. The numerical calculations reported in this paper were performed at TUBITAK ULAKBIM, High Performance and Grid Computing Center (TRUBA resources).

Appendix A. Supplementary data

Supplementary data to this article can be found online at https://doi.org/10.1016/j.matchemphys.2021.124711.

References

[1] T.H. Noh, S.W. Hwang, J.U. Kim, H.K. Yu, H. Seo, B. Ahn, D.W. Kim, I.S. Cho, Optical properties and visible light-induced photocatalytic activity of bismuth sillenites ($Bi_{12}XO_{20}$, X = Si, Ge, Ti), Ceram. Int. 43 (2017) 12102–12108.
[2] A.M. Burger, L.Y. Gao, R. Agarwal, A. Aprelev, J.E. Spanier, A.M. Rappe, V. M. Fridkin, Shift photovoltaic current and magnetically induced bulk photocurrent in piezoelectric sillenite crystals, Phys. Rev. B 102 (2020), 081113.
[3] X.J. Cao, L. Zhang, Y.X. Zhu, X. Zhang, C.N. Lv, C.M. Hou, Design and synthesis of sillenite-based micro/nanomaterials and their applications in photocatalysis, Prog. Chem. 32 (2020) 262–273.
[4] V. Marinova, R.C. Liu, S.H. Lin, K.Y. Hsu, Real-time holography in ruthenium-doped bismuth sillenite crystals at 1064 nm, Opt. Lett. 36 (2011) 1981–1983.
[5] A.T. Efremidis, N.C. Deliolanis, C. Manolikas, E.D. Vanidhis, Dispersion of electro-optic coefficients in sillenite crystals, Appl. Phys. B 95 (2009) 467–473.
[6] E.A. Barbosa, R. Verzini, J.F. Carvalho, Multi-wavelength holography in $Bi_{12}TiO_{20}$ crystals: applications in refractometry, Opt Commun. 263 (2006) 189–196.
[7] M.R.R. Gesualdi, D. Soga, M. Muramatsu, Surface contouring by phase-shifting real-time holography using photorefractive sillenite crystals, Opt Laser. Technol. 39 (2007) 98–104.
[8] L. Wiehl, A. Friedrich, E. Haussühl, W. Morgenroth, A. Grzechnik, K. Friese, B. Winkler, K. Refson, V. Milman, Structural compression and vibrational properties of $Bi_{12}SiO_{20}$ sillenite from experiment and theory, J. Phys. Condens. Matter 22 (2010) 505401.
[9] M. Isik, S. Delice, H. Nasser, N.M. Gasanly, N.H. Darvishov, V.E. Bagiev, Optical characteristics of $Bi_{12}SiO_{20}$ single crystals by spectroscopic ellipsometry, Mater. Sci. Semicond. Process. 120 (2020) 105286.
[10] Y. Belik, T. Kharlamova, A. Vodyankin, V. Svetlichnyi, O. Vodyankina, Mechanical activation for soft synthesis of bismuth silicates, Ceram. Int. 46 (2020) 10797–10806.
[11] H. Koc, S. Palaz, S. Simsek, A.M. Mamedov, E. Ozbay, Elastic and optical properties of sillenites: first principle calculations, Ferroelectrics 557 (2020) 98–104.
[12] S.A.S. Farias, J.B.L. Martins, Bonding and electronic structure of sillenites, Chem. Phys. Lett. 533 (2012) 78–81.
[13] T.M. Oliveira, C. Santos, A.F. Lima, M.V. Lalic, Antisite defect as rule for photorefractive, photochromic and photocatalytic properties of $Bi_{12}MO_{20}$ (M = Ge, Si, Ti) sillenite crystals, J. Alloy. Compnd. 720 (2017) 187–195.
[14] E. Haussühl, H.J. Reichmann, J. Schreuer, A. Friedrich, C. Hirschle, L. Bayarjargal, B. Winkler, I. Alencar, L. Wiehl, S. Ganschow, Elastic properties of single crystal $Bi_{12}SiO_{20}$ as a function of pressure and temperature and acoustic attenuation effects in $Bi_{12}MO_{20}$ (M = Si, Ge and Ti), Mater. Res. Express 7 (2020), 025701.
[15] M. Isik, S. Delice, N.M. Gasanly, N.H. Darvishov, V.E. Bagiev, Temperature-dependent band gap characteristics of $Bi_{12}SiO_{20}$ single crystals, J. Appl. Phys. 126 (2019) 245703.
[16] W.Q. Li, Z.H. Wen, S.H. Tian, L.J. Shang, Y. Xiong, Citric acid-assisted hydrothermal synthesis of a self-modified $Bi_2SiO_5/Bi_{12}SiO_{20}$ heterojunction for efficient photocatalytic degradation of aqueous pollutants, Catal. Sci. Technol. 8 (2018) 1051–1061.

[17] W. Gu, F. Teng, Z. Liu, Z. Liu, J. Yang, Y. Teng, Synthesis and photocatalytic properties of Bi_2SiO_5 and $Bi_{12}SiO_{20}$, J. Photochem. Photobiol., A 353 (2018) 395–400.
[18] S.L. Hou, R.B. Lauer, R.E. Aldrich, Transport processes of photoinduced carriers in $Bi_{12}SiO_{20}$, J. Appl. Phys. 44 (1973) 2652.
[19] M. Isik, N. Sarigul, N.M. Gasanly, Thermoluminescence characteristics of $Bi_{12}SiO_{20}$ single crystals, J. Lumin. 224 (2020) 117280.
[20] X. Li, Z. Shao, M. Zhu, J. Yang, Fundamentals of Optical Computing Technology, Springer, 2018.
[21] G. Kresse, J. Hafner, Ab initio molecular dynamics for liquid metals, Phys. Rev. B 47 (1993) 558–561.
[22] G. Kresse, J. Furthmuller, Efficiency of ab initio total energy calculations for metals and semiconductors using a plane-wave basis set, Comput. Mater. Sci. 6 (1996) 15–50.
[23] P.E. Blöchl, Projector augmented-wave method, Phys. Rev. B 50 (1994) 17953–17979.
[24] J.P. Perdew, K. Burke, M. Ernzerhof, Generalized gradient approximation made simple, Phys. Rev. Lett. 77 (1996) 3865–3868.
[25] M.C. Payne, M.P. Teter, D.C. Allan, T.A. Arias, J.D. Joannopoulos, Iterative minimization techniques for ab initio total-energy calculations: molecular dynamics and conjugate gradients, Rev. Mod. Phys. 64 (1992) 1045–1097.
[26] P. Hohenberg, W. Kohn, Inhomogeneous electron gas, Phys. Rev. 136 (1964) 864–871.
[27] W. Kohn, L.J. Sham, Self-consistent equations including exchange and correlation effects, Phys. Rev. A 140 (1965) A1133–A1138.
[28] J. Heyd, G.E. Scuseria, M. Ernzerhof, Hybrid functionals based on a screened Coulomb potential, J. Chem. Phys. 118 (2003) 8207–8215.
[29] A.V. Krukau, O.A. Vydrov, A.F. Izmaylov, G.E. Scuseria, Influence of the exchange screening parameter on the performance of screened hybrid functionals, J. Chem. Phys. 125 (2006) 224106.
[30] S. Grimme, Semiempirical GGA-type density functional constructed with a long-range dispersion correction, J. Comput. Chem. 2 (2006) 1787–1799.
[31] J.D. Pack, H.J. Monkhorst, Special points for Brillouin-zone integrations—a reply, Phys. Rev. B 16 (1977) 1748–1749.
[32] M. Methfessel, A.T. Paxton, High-precision sampling for Brillouin-zone integration in metals, Phys. Rev. B 40 (1989) 3616–3621.
[33] A. Otero-de-la-Roza, David Abbasi-Pérez, Víctor Luaña, Gibbs2, A new version of the quasiharmonic model code. II. Models for solid-state thermodynamics, features and implementation, Comput. Phys. Commun. 182 (2011) 2232–2248.
[34] W. Hanke, L.J. Sham, Many-particle effects in the optical spectrum of a semiconductor, Phys. Rev. B 21 (1980) 4656–4673.
[35] T. Sander, E. Maggio, G. Kresse, Beyond the tamm-dancoff approximation for extended systems using exact diagonalization, Phys. Rev. B 92 (2015), 045209.
[36] A.F. Lima, S.A.S. Farias, M.V. Lalic, Structural, electronic, optical, and magneto-optical properties of $Bi_{12}MO_{20}$ (M = Ti, Ge, Si) sillenite crystals from first principles calculations, J. Appl. Phys. 110 (2011), 083705.
[37] G. Surucu, A. Gencer, X. Wang, O. Surucu, Lattice dynamical and thermo-elastic properties of M_2AlB (M = V, Nb, Ta) MAX phase borides, J. Alloys Compd. 819 (2020) 153256.
[38] R. Oberschmid, Absorption centers of $Bi_{12}GeO_{20}$ and $Bi_{12}SiO_{20}$ crystals, Phys. Status Solidi 89 (1985) 263–270.
[39] D. Hou, X. Hu, Y. Wen, B. Shan, P. Hu, X. Xiong, Y. Qiao, Y. Huang, Electrospun sillenite $Bi_{12}MO_{20}$ (M = Ti, Ge, Si) nanofibers: general synthesis, band structure, and photocatalytic activity, Phys. Chem. Chem. Phys. 15 (2013) 20698–20705.
[40] W. Tang, E. Sanville, G. Henkelman, A grid-based Bader analysis algorithm without lattice bias, J. Phys. Condens. Matter 21 (2009), 084204.
[41] C. Ambrosch-Draxl, J.O. Sofo, Linear optical properties of solids within the full-potential linearized augmented planewave method, Comput. Phys. Commun. 175 (2006) 1–14.
[42] A. Gencer, A. Candan, A. Erkisi, Electronic nature, optical and mechanical properties of $M_2Pt_2O_7$ (M = Sc, Y and La) pyrochlores: a DFT study, Phys. B Condens. Matter 607 (2021) 412862.
[43] H. Fujiwara, Spectroscopic Ellipsometry Principles and Applications, John Wiley & Sons, New York, 2007.
[44] A.A. Maradudin, E.W. Montroll, G.H. Weiss, I.P. Ipatova, Theory of Lattice Dynamics in the Harmonic Approximation, Academic Press, New York, 1971.
[45] B. Onderka, The heat capacity of bismuth silicates, Thermochim. Acta 601 (2015) 68–74.